2022-04-15

X-Ray Polarimetry with the Daksha Space Telescope

B.Tech Project II

Parth Sastry

Advisor **Prof. Varun Bhalerao**

Email parth.sastry@iitb.ac.in

Abstract X-ray astronomy has come a long way since its beginnings via detectors launched on the nose cones of sounding rockets back in the 1950s. X-ray polarimetry, on the other hand, is a largely unexplored area within this otherwise mature field. With the launch of Astrosat in 2015, we have been able to obtain sensitive measurements of X-ray polarization data via the CZTI instrument onboard. With the upcoming launch of IIT-B's own *Daksha* Space Telescope, we seek to create a software pipeline in Python, to perform polarization analysis with the data to be obtained from the planned 17 onboard Cadmium Zinc Telluride (CZT) detectors. Daksha's high sensitivity and large field of view will make it the workhorse for high energy transient discovery and characterisation in the coming decade. To gauge the capabilities of Daksha and its Minimum Detectable Polarization (MDP) for various sources, we have developed a software pipeline and utilized it to analyse the capabilities of Daksha for a simulated Gamma-Ray Burst (GRB). We are currently working on using the analysis pipeline to analyse Daksha's capabilities for more sources, and are working towards a paper detailing the same.

Contents

1 Introduction

Polarization of photons is a fundamental property reflecting their nature as electromagnetic waves. A photon represents a 'packet' of electric and magnetic fields oriented perpendicular to the direction of motion, owing to which light is classified as a transverse wave. These electric and magnetic fields evolve in time according to Maxwell's equations.

Polarization describes the configuration of the electric field, by convention. The magnetic field is interrelated with the same.

All light is polarized, but different photons from a source may have different polarizations. If the distribution of polarization angles is uniform, the source radiation is said to have zero net polarization. If not, it has some net polarization. In astrophysics, generation of non-zero net polarizations requires a net deviation from spherical symmetry in either the physical structure of the source, or the magnetic field configuration of the system [1].

X-ray astronomy deals with the detection and study of X-ray radiation ($\sim$ 100keV $\sim$ 100eV) from astronomical objects. Earth's atmosphere is opaque to X-rays [2], and hence X-ray detectors have to be taken above the earth's atmosphere to make observations. X-ray observatories are typically aboard orbiting satellites to allow for long-term measurement, but early measurements were taken with instruments on-board weather balloons.

Polarization measurements of X-ray radiation from astrophysical sources contain a wealth of information about the emission mechanism behind this radiation, as well as the orientation and geometry of the structure itself. This is of particular interest to us when studying Gamma Ray Bursts (GRBs), which are highly energetic flashes of radiation primarily in the X-ray and gamma ray spectrum. The emission mechanism of Gamma Ray Bursts remains little understood [3] and polarization measurements of GRBs and GRB afterglows may provide insights into how these electromagnetic events occur. This is discussed further in Section 4.

Daksha is a proposed high-energy transients mission comprising of two satellites monitoring the entire sky in the $1 - 1000$ keV range. The primary goals of *Daksha* are to study the electromagnetic counterparts of gravitational waves, and prompt emission Gamma Ray Bursts. This project is an effort to create a software pipeline in Python to perform polarization analysis using data

to be gathered from *Daksha* in the future. It is primarily influenced by a similar pipeline created to perform polarization analysis on data gathered from Astrosat-CZTI, which is the hard X-ray detector aboard India's first astronomical satellite Astrosat [4] [5].

Section 2 talks about the theory behind how X-ray polarimetry is performed and how it's done in the case of pixellated semiconductor detectors like the Cadmium Zinc Telluride detectors aboard Astrosat and Daksha. Section 3 is a short overview of the major processing blocks that have been coded in my current Python pipeline and the other processing blocks that have been taken from elsewhere. It also talks a bit about why we've been working on coding a new pipeline when a previous pipeline already exists for Astrosat-CZTI.

Section 4 shows a comparison of results obtained via my current processing pipeline for a particular GRB, compared to data obtained from the previous pipeline. We also discuss the results we obtained for a simulated GRB and how we recovered the simulated parameters via our analysis. Section 5 concludes the report and mentions what the next steps are.

2 An Overview of X-Ray Polarimetry

2.1 Theory

Available X-ray instrumentation is able to measure the intensity of X-rays (the number of photons per unit time), the energies of X-rays (via conversion of that energy to charge or heat), and the positions of X-rays or, more precisely, the positions at which an X-ray deposits charge via interactions. Since X-ray polarization cannot be measured directly, the X-rays must first undergo some interaction that converts the polarization information to a directly measurable quantity, typically intensity or position [6].

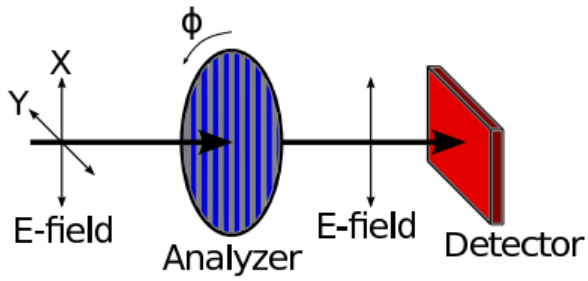

Figure 1: *Polarization Analyzer : A linear polarization analyzer is rotated and the associated detector records the intensity of photons (counts) at each angle as a modulation curve. Image Credits: [1]*

Consider a rotating polarization analyzer shown in Figure 1. As the analyzer is rotated, the intensity of photons detected changes. The resulting histogram of counts versus rotation angle is called the Modulation Curve, which in general has the form -

$$S(\phi) = A + B\cos^2(\phi - \phi_0) \tag{1}$$

here, ϕ_0 is the polarization angle at which maximum intensity is recorded.

The method of obtaining the previously described modulation curve changes depending on the polarimeter and the physical processes used for polarization

measurement. The principle behind polarimetry using the Cadmium Zinc Telluride Detectors used in Astrosat and Daksha is that of Compton scattering of high-energy photons with electrons present within the detector. Polarimeters based on this principle are called Compton polarimeters.

2.1.1 Compton Polarimeter

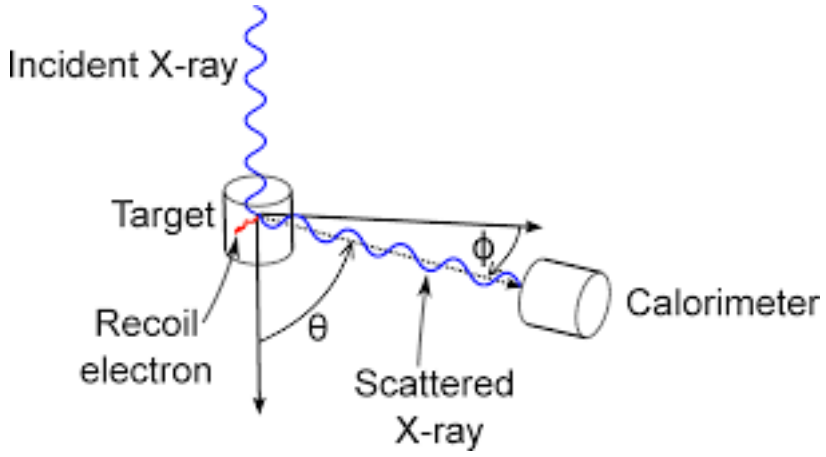

Figure 2: *Working Principle behind any Compton Polarimeter. Image Credits: [1]*

At energies above a few tens of keV, Compton scattering is the dominant interaction of X-rays with matter. When the X-ray energy is an appreciable fraction of the rest mass energy of an electron, the electron will recoil during the interaction, taking energy from the photon. The basic working of any Compton Polarimeter is shown in Figure 2.

The cross-section of scattering is given by the Klein-Nishina formula -

$$\frac{d\sigma_C}{d\Omega} = \frac{r_e^2}{2}\left(\frac{E'}{E}\right)^2\left[\frac{E'}{E} + \frac{E}{E'} - 2\sin^2\theta\cos^2\phi\right] \tag{2}$$

where r_e is the classical electron radius, E is the initial photon energy, E' is the final photon energy, and we have averaged over the polarization of the final photon [7]. ϕ is measured with respect to the incident polarization angle ϕ_0. For scattering angles near 90°, the azimuthal distribution of the scattered photon is strongly dependent on the X-ray polarization, making Compton scattering an

effective tool for polarization analysis. The dependence of $\frac{d\sigma_C}{d\Omega}$ on ϕ is shown in Figure 3.

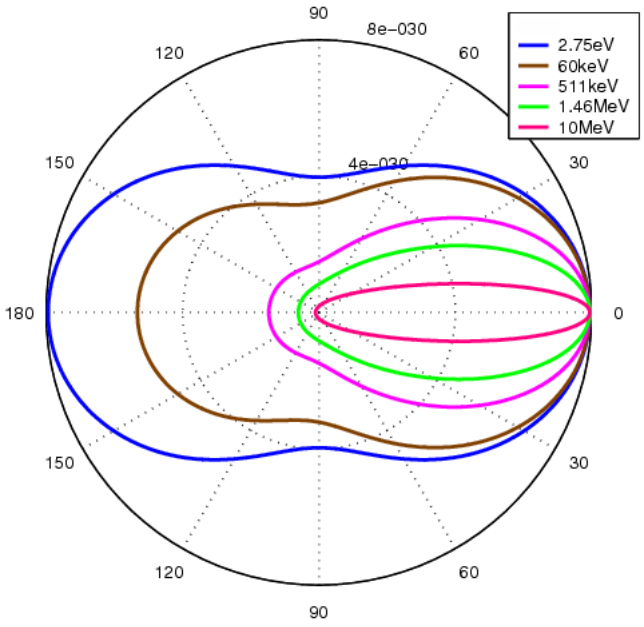

Figure 3: *The Klein-Nishina cross section as a function of energy, plotted on a polar plot. The angle here is ϕ. Image Credits : User Dscraggs on Wikipedia*

The Klein-Nishina formula is difficult to fit for when the source is off-axis (θ is largely different from 90°). On top of this, the method by which we aim to minimize the impact of off-axis sources impacting our analysis (discussed in subsection 2.5.2) doesn't work as well when we assume the underlying distributions follows Equation 2 strictly. To perform Compton Polarimetry, we assume that this deviation due to θ doesn't impact the modulation curve by a large amount, and we can assume a $cos(2\phi)$ distribution for the modulation curve, the form of which is given by -

$$C(\phi) = A\,cos(2(\phi - \phi_0 + \pi/2)) + B \tag{3}$$

The modulation amplitude for this equation is expressed as -

$$\begin{aligned}\mu &= (C_{max} - C_{min})/(C_{max} + C_{min}) \\ &= ((A+B) - (B-A))/((A+B) + (B-A)) = A/B\end{aligned} \tag{4}$$

Given a modulation curve, we can obtain ϕ_0, A and B via fitting via Chi-Square Minimization. The degree of polarization or polarization fraction p, which represents the fraction of incident photons which are polarized, can be obtained from the observed μ value as $p = \mu/\mu_{100}$. Here, μ_{100} is the modulation amplitude as measured for a 100% polarized beam.

However, this measurement is impacted via the addition of chance coincidence events from the background (which are expected to be unpolarized). In this case, the actual p will be larger than the computed p by some fraction. For a polarimeter with some μ_{100}, a background count rate $R_{\rm bkg}$ independent of rotation angle, the polarization fraction of a source with modulation amplitude a and count rate $R_{\rm src}$ is -

$$p = \frac{a}{\mu_{100}} \frac{R_{\rm src} + R_{\rm bkg}}{R_{\rm src}} \tag{5}$$

In designing an X-ray polarimeter, it is essential that the system (analyzer, detector and telescope) can reach sufficient statistical accuracy for the measurements required. The traditional figure of merit is the 'Minimum Detectable Polarization' (MDP) [8].

The polarization fraction, p, is a non-negative quantity. Any particular measurement of p will produce a value greater than 0. The MDP is the largest fluctuation expected to occur with a probability of 0.01. Equivalently, the MDP is the smallest polarization that can be detected at a 99% confidence level. The MDP for an observation of duration T is -

$$\text{MDP} = \frac{4.29}{R_{\rm src}\mu_{100}} \sqrt{\frac{R_{\rm src} + R_{\rm bkg}}{T}} \tag{6}$$

Usually, a scientifically useful polarization measurement entails determination of both p and ϕ_0. This is a joint measurement of two parameters and requires additional statistics beyond those suggested by the MDP [9], however we don't go into those in this report or project.

2.2 Semiconductor X-Ray Detectors

Semiconductor detectors have developed rapidly in recent years and are now used in a variety of fields, including X-ray and Gamma ray astronomy, nuclear physics and nuclear medicine. In comparison with gas detectors and scintillators, they have good energy resolution and can form much more compact systems.

The typical operation of semiconductor detectors is based on collection of the charges, created by photon interactions, through the application of an external electric field. The choice of the proper semiconductor material for a radiation detector is mainly influenced by the energy range of interest. There are three primary interactions of X-rays and Gamma rays with matter that are important when considering X-ray measurements. -

1. **photoelectric absorption** : the interacting photon transfers all its energy to an atomic electron
2. **compton process** : the interacting photon transfers only a fraction of its energy to an outer electron, producing a hot electron and a degraded photon
3. **pair production** : interacting photon with energy above a threshold energy interacts within the Coulomb field of the nucleus producing an electron and positron pair

Consider a simple planar detector - a slab of a semiconductor material with metal electrodes on the opposite faces of the semiconductor - Figure 4. Photon interactions produce electron-hole pairs in the semiconductor volume through the discussed interactions. The interaction is a two-step process where the electrons created in the photoelectric or Compton process lose their energy through electron-hole ionization.

The number of electron-hole pairs generated is proportional to the photon energy. If E is the incident photon energy, the number of electron-hole pairs generated is -

$$N = \frac{E}{w}$$

here, w is the average electron-hole pair production energy. The generated

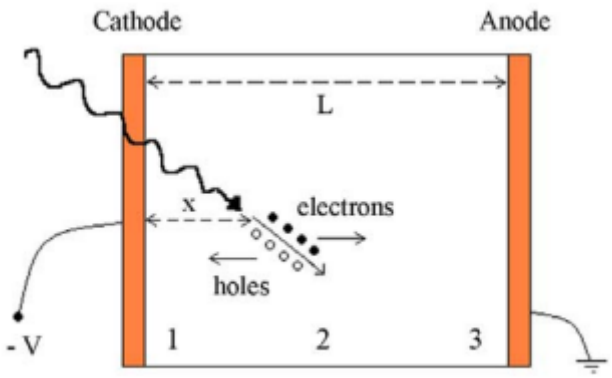

Figure 4: *Planar Configuration of a semiconductor detector. Electron-hole pairs generated are swept away to the appropriate electrode via an external electric field. Image Credits : [10]*

charge Q is thus $Q = Ne = Ee/w$ [10]. Measurement of this generated charge at the anode (anode, because electrons move much faster than the corresponding holes, allowing us to take readings faster) allows us to calculate the incident energy E of the photon. Arranging multiple detectors in a tiled configuration allows us to create an ensemble pixellated detector.

For our polarization analysis, we utilize Compton Scattering events that occur in medium-energy X-Rays. The detectors that we use to detect these photons must, therefore, be sensitive to photons in this energy range. The detectors used in Daksha and Astrosat are Cadmium Zinc Telluride (CdZnTe, or CZT) detectors, where the semiconductor material used is $Cd_{1-x}Zn_xTe$. These detectors are sensitive to photons in the energy range of 20-200 keV. The CZT detectors developed for AstroSat and Daksha are capable of time-tagging events with a resolution of $< 10\mu s$, allowing for identification of incident and scattered photons. These features make them suitable for polarization studies.

2.3 Compton Polarimetry with Pixellated Detectors

Compton polarimetry with pixellated detectors works with similar ideas in mind as standard Compton polarimetry discussed in 2.1.1. The major difference

in the case of pixellated detectors, of course, is that we do not have scattering counts for continuously varying ϕ values. The incident photon transfers a fraction of its energy to the recoil electron, which is detected at the anode of the semiconductor detector at the site of incidence (*incident pixel*). A larger part of the photon's energy is transmitted to the scattered photon, which is detected within the detector in some other pixel (*scattered pixel*).

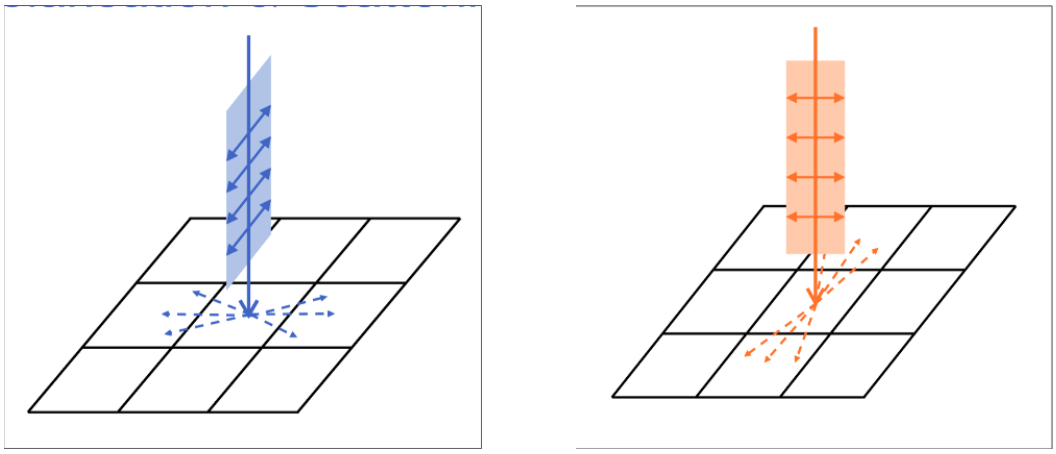

Figure 5: *Schematic representation of Compton scattering process in pixelated detectors. The solid arrows are showing the direction of the electric field vector, and the broken arrows are showing the radiation produced by oscillating electron on the detector plane.*

2.3.1 Compton Scattering Events

To try and arrive at an angular distribution of scattering, we treat scattering events occuring in specific pixels as occuring in discrete angular bins, and generate a histogram based off of that. This is shown in Figure 6. There are a couple of points to note here -

1. the detection of the Compton scattered photon is expected to occur at the same time as the detection of the incident photon since photon travel time is negligible. This gives us the definition of a **double event** as detection events occurring within the duration of the resolution window of the internal detector clock
2. the Compton scattered photon isn't expected to travel far from the scattering site before getting absorbed, so we only consider double events

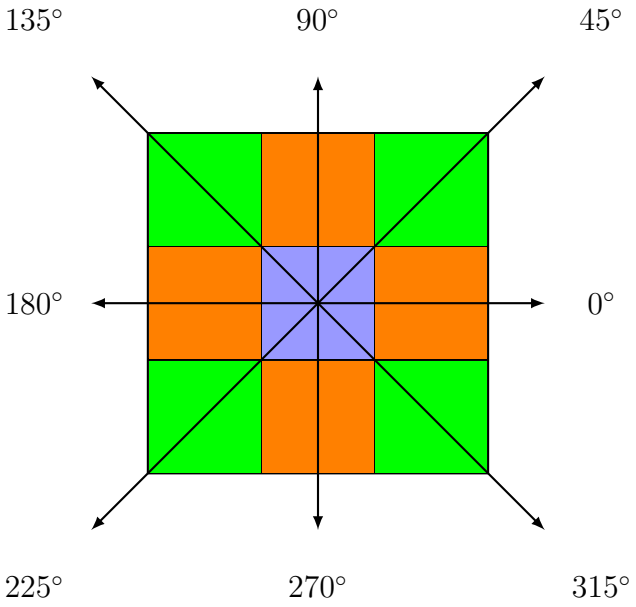

Figure 6: *Central pixel in purple and neighboring pixels. Simultaneous events in these neighboring pixels constitute a valid double event*

occurring within **adjacent pixels** to avoid the chance coincidence events that are going to occur (two independent photons arriving within the detector resolution window at different pixels)

3. despite imposing the neighboring pixel criteria, you still observe some chance coincidence events, and thus we impose a third criteria comparing the energies of the two events and imposing a limit on the total energy of the incident photon. This is the **Compton criteria**

For a true Compton scattering event, energy of the scattered photon is always greater than the recoil electron energy for incident photon energies < 280 keV. Furthermore, we only select incident and scattered photons lying within the energy range of $20 - 200$ keV having total energy 100 keV $\leq E_{tot} = E_{scattered} + E_{incident} \leq 400$ keV. These event energy criteria and total energy criteria help us make sure we only select true Compton Events (since Compton Scattering occurs mostly among medium energy X-Rays), and that we do not select chance photoelectric absorption, pair production, Bremsstrahlung, etc. events.

For lower energy of the incident photons and scattering angles around 90°, the

ratio of the energy of the scattered photon and the recoil electron is ≥ 2. This helps us to further weed out chance coincidence events from true scattering events.

To summarize - double events occurring in adjacent pixels (Figure 6) that satisfy the Compton Criteria are valid Compton events. Depending on which adjacent pixel the scattering occurred in, we assign this Compton event an **angular bin** ranging from 0° to 360° in increments of 45°. This gives us the observed angular distribution, or *histogram* of Compton events that are seen in our data. There are corrections to be made to this distribution before obtaining the modulation curve, which are discussed in Subsection 2.5

All these results are taken from the PhD thesis of Dr. Tanmoy Chattopadhyay [11] who was responsible for coming up with this pipeline to perform X-ray polarimetry with CZT detectors. Dr Chattopadhyay also coded the pipeline to perform this analysis using the CZT detectors aboard Astrosat, which the current Daksha pipeline is expected to build upon.

2.4 Astrosat and Daksha

Before we move on to discussing what the Astrosat mass model is, why is it required and how does it relate to the Daksha mission, we discuss the two satellites to see what the instruments obtaining our data are, and what payloads do we use for our polarization studies.

2.4.1 Astrosat

Astrosat is a multi-wavelength astronomy mission launched on September 28, 2015. A schematic of the satellite is shown in 7. It is India's first space observatory and has 5 astronomy payloads -

1. twin 38-cm **Ultraviolet Imaging Telescopes (UVIT)** covering Far-UV to optical bands
2. three units of **Large Area Xenon Proportional Counters (LAXPC)** covering medium energy X-rays from 3 to 80 keV
3. a **Soft X-ray Telescope (SXT)** covering the energy range 0.3-8 keV

4. a **Cadmium-Zinc-Telluride coded-mask imager (CZTI)**, covering hard X-rays from 10 to 150 keV
5. a **Scanning Sky Monitor (SSM)** that is placed on a rotating platform to scan the available sky once every six hours in order to locate transient X-ray sources

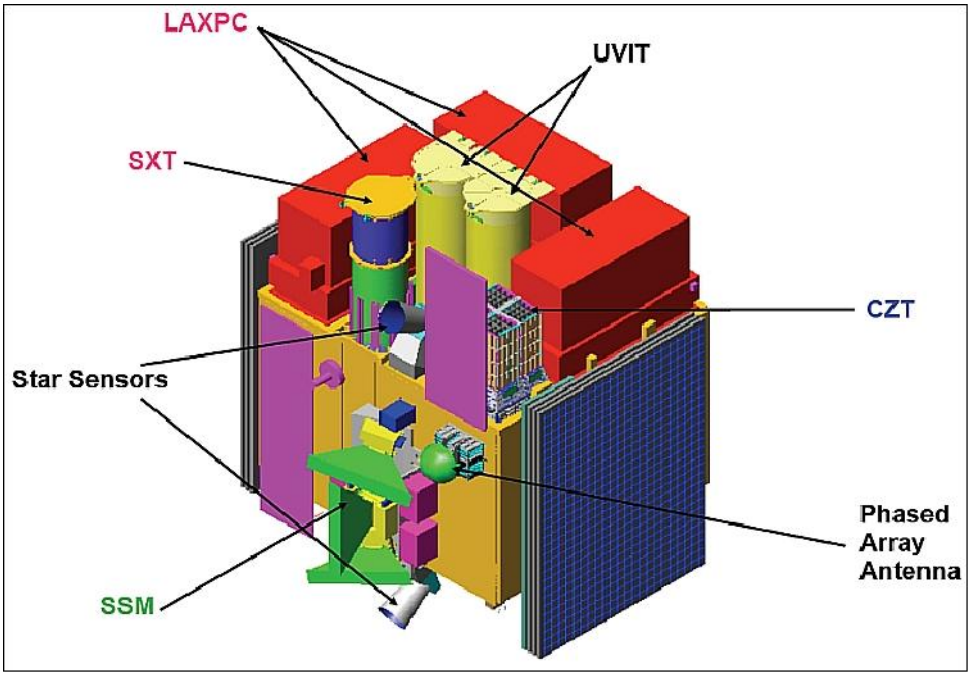

Figure 7: *Illustration of the AstroSat spacecraft and its instrument complement. Image Credit: ISRO*

The CZTI is of primary interest to us, since it covers the hard X-ray energy range where GRBs (Gamma Ray Bursts) and other transient sources are detected. As stated in the Introduction, an IDL (Interactive Data Language) pipeline already exists to perform polarization analysis using CZTI data.

As validation of our pipeline for Daksha, we made sure to be able to perform polarization analysis of transient sources detected using CZTI via our pipeline, allowing us to compare results and make sure the finished software could still be used while Daksha is in development, on CZTI data.

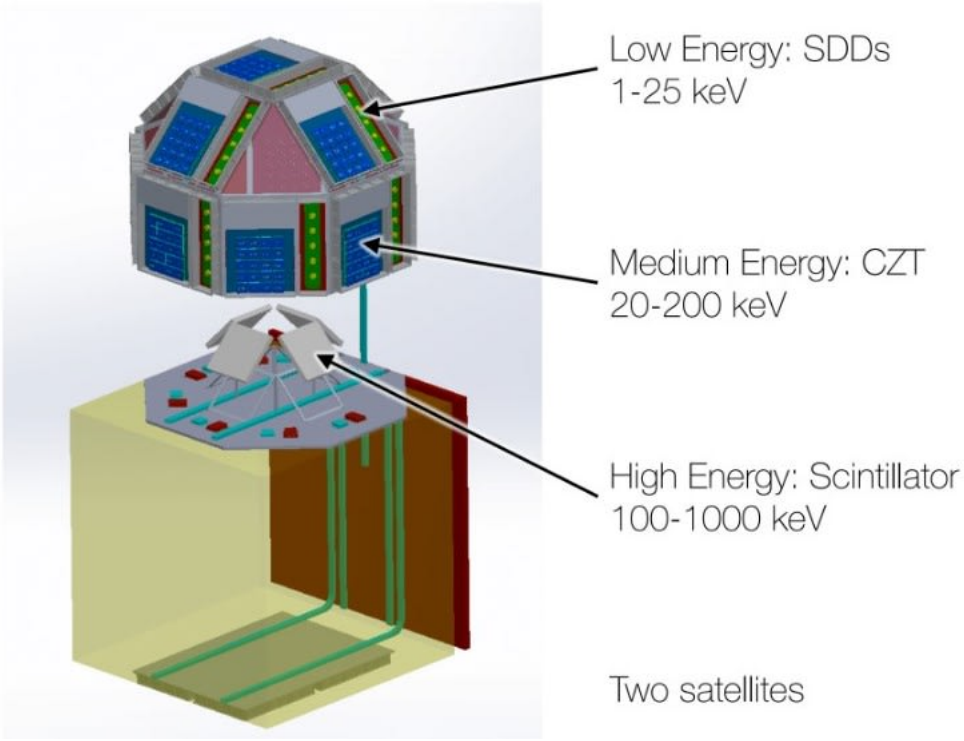

Figure 8: *Proposed design of Daksha. Image Credit: Varun Bhalerao, Santosh Vadawale and the Daksha team*

2.4.2 Daksha

Daksha is a proposed space telescope being developed by IIT-Bombay for detecting high energy counterparts to gravitational wave sources. It will be an order of magnitude more sensitive than any existing mission. It will cover the energy range from 1 keV to ≥ 1 MeV, reaching a sensitivity higher than the *Neil Gehrels Swift Observatory*. Two satellites orbiting on opposite sides of Earth will ensure continuous coverage of the entire sky. [1]

Daksha will have 17 CZT detectors onboard, compared to Astrosat-CZTI's 4 CZT detectors, which will allow us to perform polarization analysis on detected X-ray transients. With more detectors, and a mission comprised of two satellites, Daksha is expected to have higher sky coverage than Astrosat. With its CZT detectors being in different orientations, it is not only expected to detect more transients than Astrosat, but also to help in quantifying any systematic errors in

[1] https://www.star-iitb.in/research/daksha

transient polarisation measurements, an advantage over the coplanar quadrants of Astrosat-CZTI.

2.5 Obtaining Polarization Measurements

There are two primary ways we are aiming to obtain polarization measurements of a given source - 1) fitting the modulation curve to a cosine function, and 2) template matching. For both methods, the starting point is background subtracted azimuthal histograms of the selected Compton events. Azimuthal scattering angles in the detector plane are computed for each pair of Compton events and an eight-bin histogram is generated.

In addition to the raw histograms, azimuthal histograms for unpolarized and 100% polarized beams incident at the same direction as in observations, with the same energy spectrum are required for analysis via both approaches. Generation of these simulated histograms is where the Mass Model comes in.

2.5.1 The Mass Model

The mass model is something that was developed for Astrosat to perform simulations of the passage of radiation through the satellite, and to simulate light-matter interactions within the same. This is done with the help of the `GEANT4` toolkit for particle, photons and matter interactions [2]. The mass model is a reproduction (with accurate chemical and geometrical properties) of the Astrosat satellite, within `GEANT4` [12].

Individual photons in incoming radiation can then be tracked and simulated as they travel through the satellite and are detected within the detectors. This allows us to simulate the interaction of incoming radiation with the satellite, to yield the final energies (spectrum) and positions (Detector Plane Histogram, or DPH) of photons incident on the detector [13].

The full implementation of how the mass model is implemented for Astrosat is detailed in reference [13]. The Astrosat mass model allows us to simulate what would happen if we placed some EM source at a specific orientation to the satellite. It's a complex simulation which involves individually tracking the interaction of millions of photons with the particles of the satellite, allowing

[2] https://geant4.web.cern.ch/

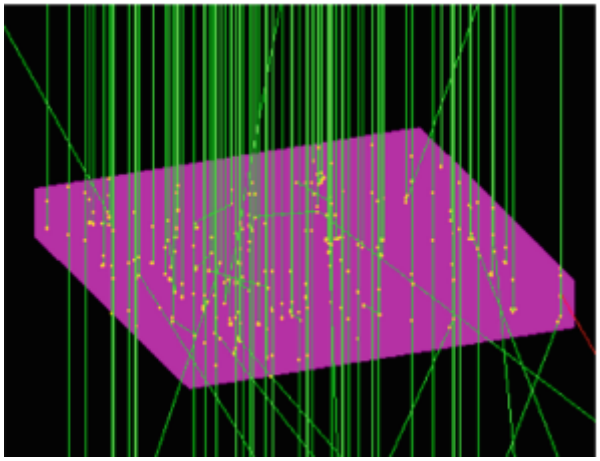

Figure 9: *Simulated diagram for a CZT module (40 mm × 40 mm × 5mm). The module is shined uniformly by X-ray photons shown in green. Image Credits: Tanmoy Chattopadhyay [11]*

us to look at what the angular distributions of Compton events would look like if the simulated source was of same spectrum and incident at the same off-axis angle as the detected source, for different polarization angles and fractions.

2.5.2 Modulation Curve

When computing the azimuthal histogram, we glossed over the fact that the angular bins we assign to each neighboring pixel are unequal. It is readily apparent that the edge pixels (colored orange in Figure 6) occupy a larger angular size than the corner pixels (colored green in Figure 6). This will skew the observed angular distribution drastically in favor of the 0°, 90°, 180° and 270° bins, while reducing the counts in the other bins.

There's another problem. When the event being observed is off-axis, the angular distribution is further complicated, because of the break in symmetry in the pixel geometry with respect to the incident photon direction. The observed distribution will be some form of projection of our cosine function onto the detector plane.

However, both these effects can be taken care of by normalizing the azimuthal distribution by that for 100% unpolarized radiation, of the same spectrum

and incident at the same off-axis angle as the source. Thus the observed modulation pattern has to be normalized using the similar modulation pattern for an unpolarized beam. This unpolarized beam is simulated via mass model simulations. [14].

Let H_i^{obs} be the observed histogram, and H_i^{unpol} be the simulated unpolarized histogram. Let $H_i^{pol}(\psi)$ be the simulated 100% polarized histogram for the sky polarization angle ψ. All histograms are normalized such that the mean number of counts is 1. Following this -

- Normalize the observed histogram with unpolarized histogram to obtain the modulation curve $M_i^{obs} = \frac{H_i^{obs}}{H_i^{unpol}}$
- Fit M_i^{obs} with Equation 3 to obtain A, B and ϕ_0
- Compute $\mu = A/B$
- From the fitted phase angle ϕ_0, compute sky plane polarization angle ψ_0 (what this means is detailed further in Section 4)
- Obtain the simulated histogram for 100% polarized beam H_i^{pol}, follow the preceding steps to compute μ_{100} for 100% polarized beam
- To get simulated histogram for 100% polarized beam, instead of using the estimated sky plane polarization angle from the fitted ϕ_0, we obtain μ_{100} values over a grid of sky plane polarization angles and interpolate to get the μ_{100} for our observed polarization angle
- Estimate the polarization fraction p using Equation 5.

2.6 Template Fitting

Let H_i^{obs} be the observed histogram, and H_i^{unpol} be the simulated unpolarized histogram. Let $H_i^{pol}(\psi)$ be the simulated 100% polarized histogram for the sky polarization angle ψ. All histograms are normalized such that the mean number of counts is 1. In this case, we create a grid of $H_i^{pol}(\psi)$ histograms for ψ every 5 (or 10) degrees.

- A library of template histograms $H_i^{sim}(p_m, \psi_n)$ for polarization fraction p_m and polarization angle ψ_n (sky plane) are obtained by weighted addition - $H_i^{sim}(p_m, \psi_n) = p \cdot H_i^{pol}(\psi_n) + (1 - p_m) \cdot H_i^{unpol}$. This library exists over a

grid of ψ_n, p_m values. Histograms for intermediate polarization angles can be obtained via interpolation.

- Compute the Chi-Squared value for the difference between observed and simulated histograms -

$$\chi^2(p_m, \psi_n) = \sum_{i=0}^{7} \left(\frac{H_i^{obs} - H_i^{sim}(p_m, \psi_n)}{\sigma_i^{obs}} \right)^2 \tag{7}$$

- Best-fit PF and PA are where this χ^2 value is minimized. Contours of $\Delta\chi^2$ provide two-parameter confidence intervals for PA and PF.

2.7 The Daksha Mass Model

The Daksha team has been working on a mass model for Daksha, which will be used for sensitivity calculations, localization, spectroscopic analysis and polarimetric measurements and simulations. The Daksha mass model will give us the histograms we require for any of our previous analyses.

For our current simulated sources, we have used the mass model for individual detector boxes suspended in space. As the mass model grows in complexity to accomodate all the various materials within the Daksha satellite, these simulations will become more and more accurate, and lead to more comprehensive results.

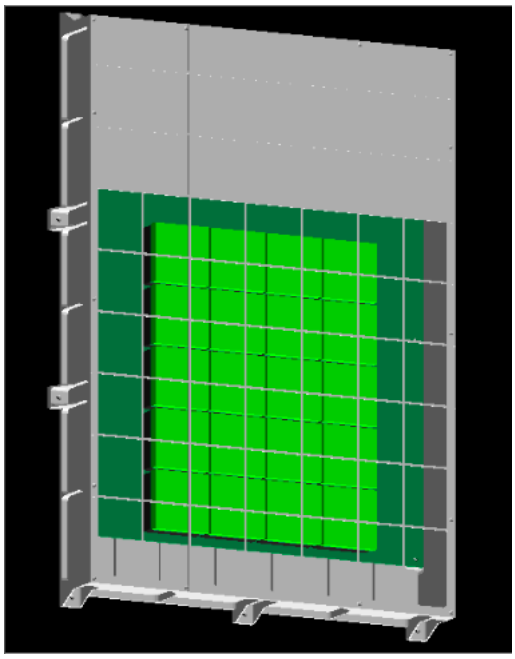

Figure 10: *The picture shows the graphical rendering of a single ME box mass model. The CZT modules (Light Green squares) are coded as accurately as possible. The front end PCB and the box cover are imported using CAD models. Credits : Sujay Mate*

3 Data Processing Pipeline

A schematic detailing the polarization analysis pipeline is shown below

As stated earlier, there exists an IDL pipeline to perform each of the tasks mentioned in this flowchart. The choice of language is a consequence of when Astrosat was being planned, when IDL was the preferred language of the astronomy community, and support for open source languages like Python wasn't as prevalent, particularly for astronomical data analysis.

With the advent of Python packages like `astropy` and the general shift of the astronomy community towards open-source and freely available software, unlike IDL which is proprietary, the decision was made to write this pipeline for Daksha (or at least, some parts of it) in Python. That is the goal of this project. We go over the important steps being recreated once -

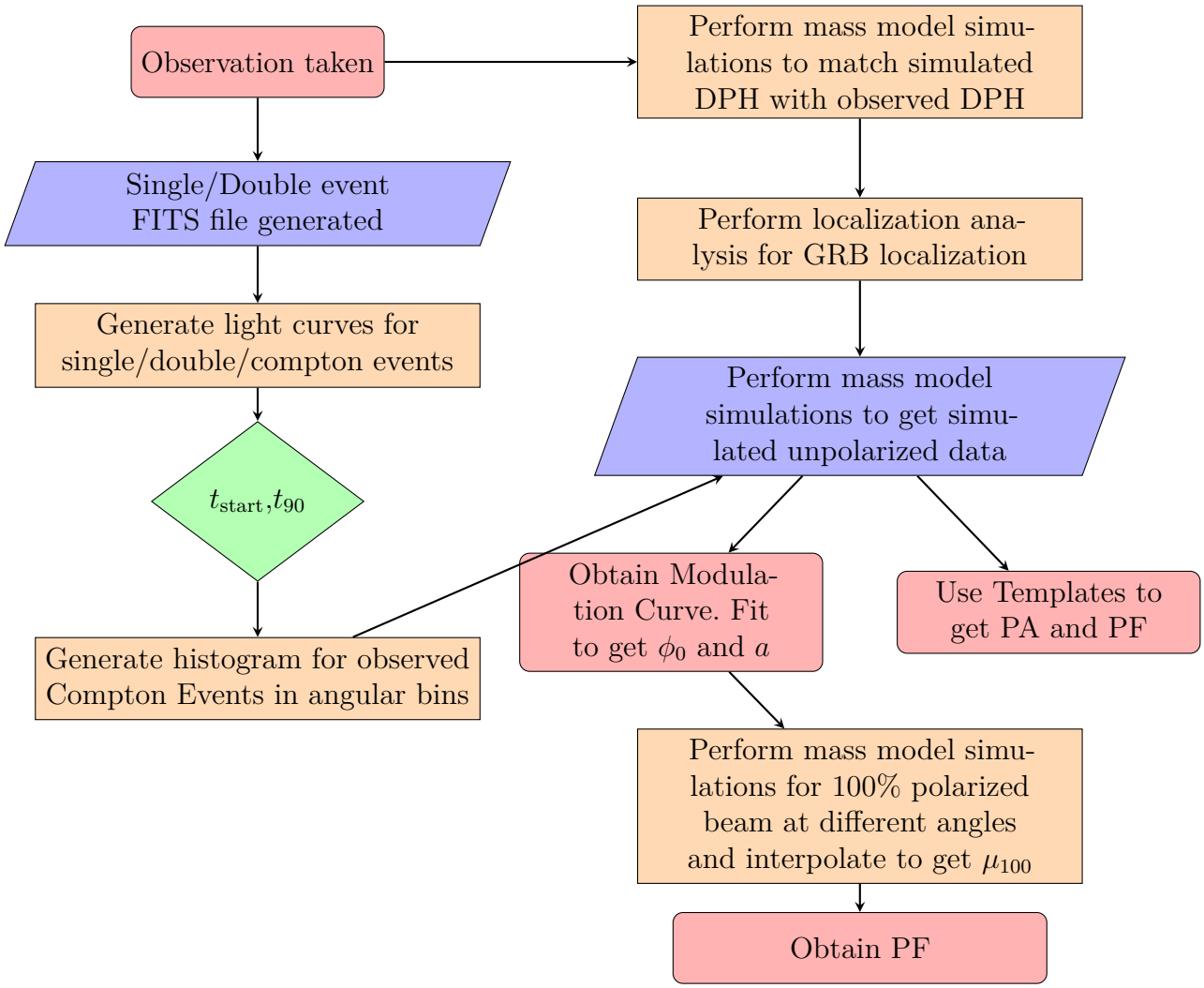

Figure 11: *Data Processing Pipeline*

1. **Generate light curves for single/double/compton events** - data arrives in the forms of processed FITS files into this pipeline. Single event files are used to generate a histogram (or light curve) of single event counts during the duration of the GRB. Likewise for double event files, which are processed to find *valid double events* as occurring in adjacent pixels, and *valid compton events*, those of which fulfill the Compton criteria. The histograms (light curves) of these are plotted and saved

2. $\mathbf{t_{start}}$, $\mathbf{t_{90}}$ - t_{start} or the trigger time refers to the start time of the GRB.

This is something that can be selected by the user based on the light curve observed. t_{90} is the point of time before which 90% of the total incident photons have been detected. This is something that can be auto-computed by the pipeline, or can be tweaked by the user.

3. **Generate histogram for observed Compton Events in angular bins** - once we have found valid Compton events among the observed double events, we generate our observed angular distribution according to the process detailed in subsection 2.3.1

4. **Obtaining the Modulation Curve/Template Fitting** - after extensive mass model simulations to find the location of the GRB, we simulate the histograms for 100% polarized beams for different PA values. From here on, we either perform Template Fitting as detailed in Subsection 2.6 or obtain the corrected Modulation Curve, and then fit to get the PA and PF as detailed in Subsection 2.5.2.

As of this stage, the current pipeline is able to get a modulation curve via normalization with the output of the Astrosat mass model. The results that the current pipeline generates for a sample GRB we chose (GRB 160325A) almost match exactly to what the old pipeline generated. I'd shown this in the previous report. Following this, we performed simulations for a source GRB to simulate what Daksha *would* have observed on 3 of its faces, to see whether these methods allow us to recover the simulated parameters. We show the results for our simulated GRB, and explain the methodology in the next section.

4 Current Implementation and Results

4.1 Measuring GRB Polarization

4.1.1 What are GRBs?

We have discussed GRBs fleetingly before as the X-ray transient sources we are hoping to study with Daksha. GRBs or Gamma Ray Bursts are immensely energetic explosions observed in distant galaxies. The identification of the progenitors of these explosions is challenging and an object of current study.

As of recent years, LIGO has been detecting gravitational waves via mergers of neutron stars and black holes in far-away galaxies. Finding the electromagnetic counterparts to these gravitational wave sources, which are thought to be GRBs in the case of binary neutron star mergers, would provide us with a wealth of information on the processes that happen during these mergers and their mechanisms of radiation.

Detecting GRBs and analysing the spectrum of their radiation is important, and this project serves to code part of a pipeline which would allow future users of *Daksha* data to analyse and make new insights into these awesome objects.

4.1.2 Are GRBs polarized?

Depends.

Radiation from GRBs is expected to be from outflows moving towards us with relativistic speeds. The emission mechanism behind prompt emission is little understood and there exist various theories for the same. In some mechanisms for emission, polarization is expected to be high and in other cases, it's supposed to be dependent on the geometric viewing angle. Toma et al. (2009) [15] have shown that the statistical distribution of GRB polarization may lift the degeneracy of these theoretical models. Thus, analysing GRB polarization might help us solve the mystery of the way these explosions occur.

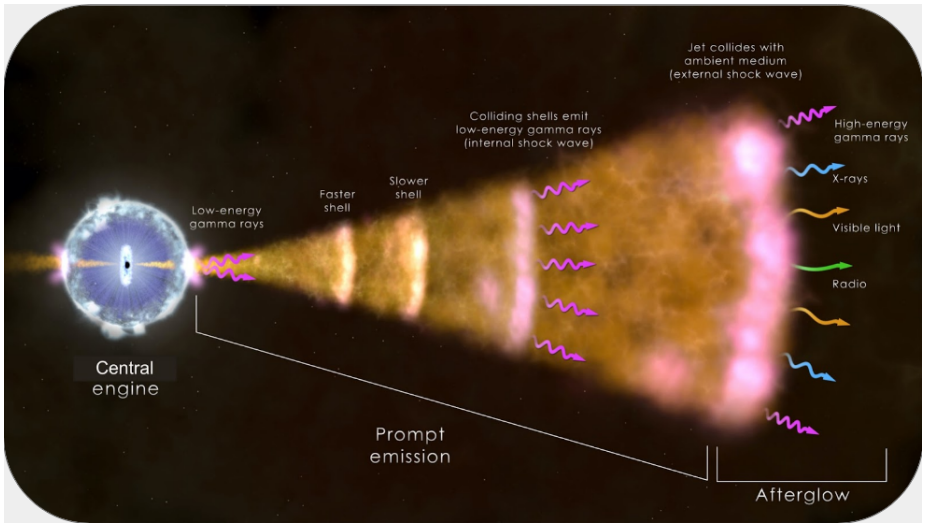

Figure 12: *Schematic of a GRB*

4.2 Simulating a GRB

4.2.1 Which GRB?

We simulated GRB17101A for our polarization analysis. We chose this GRB because GRB171010A is one of the brightest GRB observed with AstroSAT/CZTI, having 71364 total counts, and 3702 Compton counts. GRB171010A was found to be 40% polarized with polarization angle 42° (CZTI local coordinates, different from sky plane polarization angle). (Vikas et. al. 2019)

4.2.2 Setup

We generate "realistic" data for the GRB by carrying out GRB + background simulations. Using the GRB position, trigger time and the pointing direction of Daksha at trigger time, we estimate the angle of the GRB in local frame of Daksha. We select three faces of Daksha which would detect most number of photons from the GRB and simulate the GRB individually in the local coordinates of each face. The simulations are done at discrete energies between 100 keV to 1 MeV with fixed number of photons and the detected events are normalised using the GRB spectral parameters.

By this, we mean that we carried out monoenergetic simulations at energy

steps from 100 keV to 1 MeV for a constant number of incident photons on each face. To match this horizontal GRB spectrum to the observed GRB spectrum, we scaled down the number of Compton Events observed in each bin by a factor equivalent to the ratio between observed counts/cm^2 between two energy bins with the number of photons per cm^2 that we simulated for that energy value.

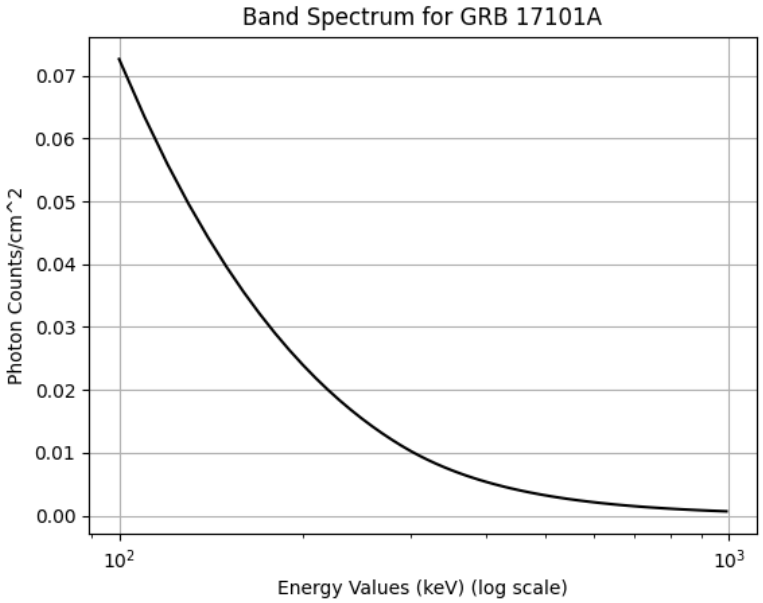

Figure 13: *Band Spectrum for parameters obtained from GRB17101A*

Previous estimates of Daksha background show that the most dominant background component will be the Cosmic X-ray Background and its reflection from the Earth's atmosphere. Hence we take a spectra which is addition of these component and neglect other components. The detected events are then normalised based on the input background spectra. This constitutes the background histograms added to the simulated source histograms to mimic real-world data.

4.2.3 Histograms

The histogram for a certain PF (Polarization Fraction) is generated from simulations by mixing as -

$$f(\phi) = PF \times f(\phi)_{100\%\ \text{pol}} + (1 - PF) \times f(\phi)_{\text{unpol}} + f(\phi)_{\text{bkg}} \tag{8}$$

where $f(\phi)$ is the azimuthal distribution of Compton Events over our 8 angular bins.

The GRB PA - 172.8° in ICRS coordinates, was converted to local sky coordinates for each face, which was recovered via interpolation on ϕ_0. A figure matching the local sky PA versus fitted ϕ_0 was used to narrow down the GRB local sky PA for each face. We recovered the parameters that the GRB was simulated with.

4.3 Obtained Modulation Curves

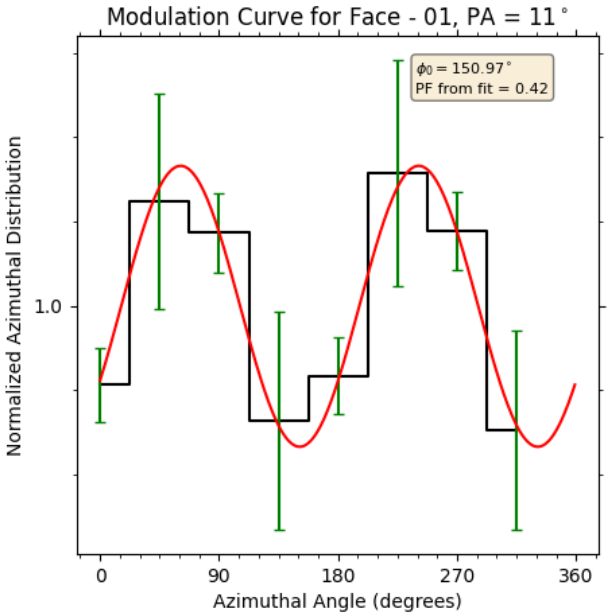

Figure 14: *Corrected Histogram in black, best-fit modulation curve in red. GRB local sky PA was* 11° *for Face 1*

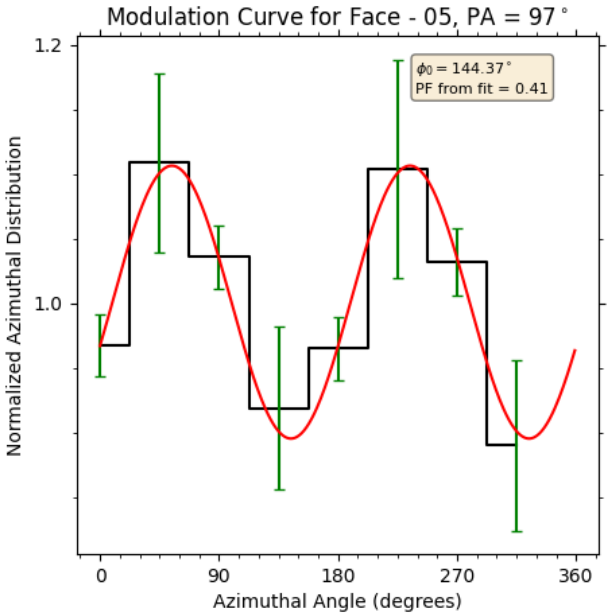

Figure 15: *Corrected Histogram in black, best-fit modulation curve in red. GRB local sky PA was* 97° *for Face 5*

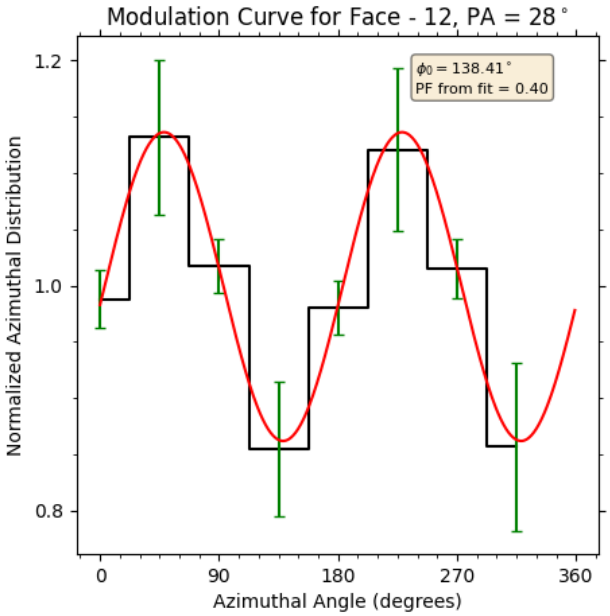

Figure 16: *Corrected Histogram in black, best-fit modulation curve in red. GRB local sky PA was* 28° *for Face 12*

4.4 Re-Obtaining the local Sky PA

We conducted 100% polarized beam simulations over a grid of local sky PAs for each face to get the relationship between Sky PA for a face and computed ϕ_0 values. The plots, and the local sky PA interpolated for each face is shown below as figures and a table.

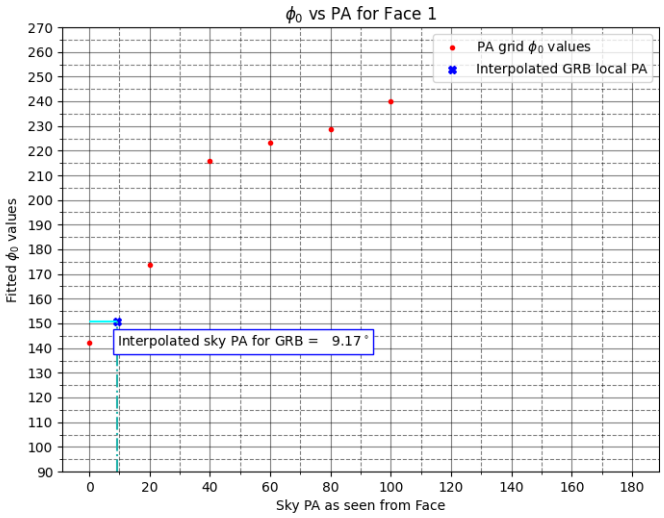

Figure 17: *Relation between fitted ϕ_0 and local sky PA for Face 1. Recovered PA is mentioned in the plot.*

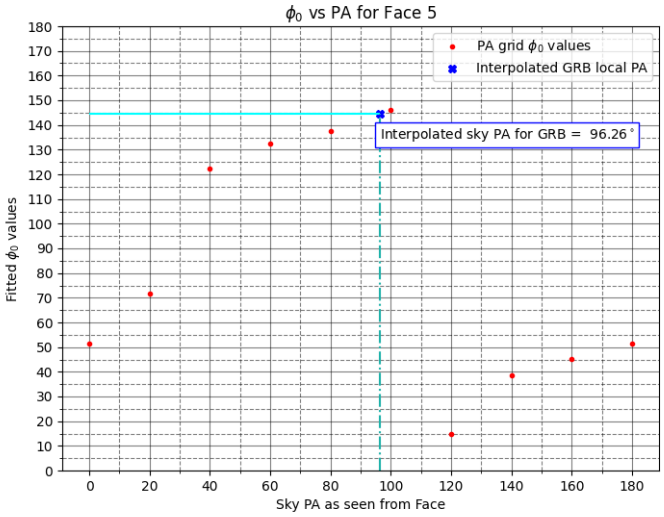

Figure 18: *Relation between fitted ϕ_0 and local sky PA for Face 5. Recovered PA is mentioned in the plot.*

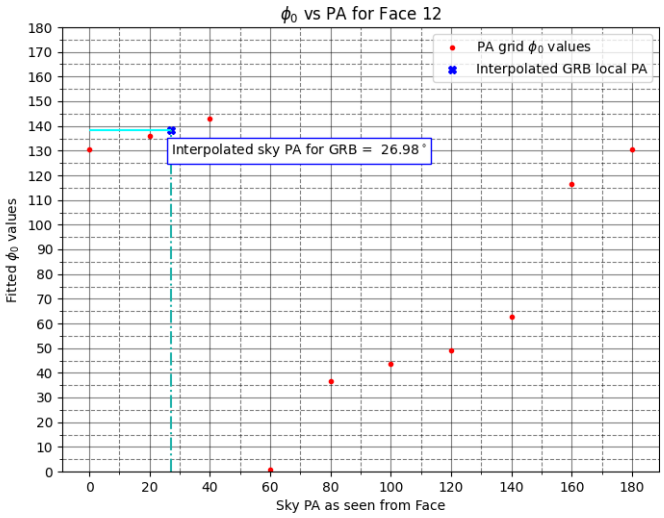

Figure 19: *Relation between fitted ϕ_0 and local sky PA for Face 12. Recovered PA is mentioned in the plot.*

Face Num	Input PF	Fitted PF	Local Sky PA	Interpolated Local Sky PA
1	0.4	0.42	11	9.17
5	0.4	0.41	97	96.26
12	0.4	0.40	28	26.98

Table 1: *Recovered Parameters vs Actual Parameters*

5 Next Steps and Conclusion

5.1 Template Matching

We have recovered the simulated GRB parameters via fitting the Modulation Curve to a cosine function. The next step is to recover these parameters via Template Matching, to see if this method works just as well. The code for this is already in place, and we'll be testing this out on the previously simulated GRB soon.

5.2 Simulating more GRBs

Our plan is to simulate 5-10 GRBs by the end of May, and to check if our pipeline recovers the parameters for these simulated GRBs well. I aim to perform the analysis for these using Template Matching, and thus getting this part of the code verified on our sample simulated GRB is crucial.

Simulating these GRBs is also instrumental to performing MDP calculations for Daksha, an important metric to gauge Daksha's polarimetric sensitivity.

5.3 MDP calculations for Daksha

$$\text{MDP} = \frac{4.29}{R_{\text{src}}\mu_{100}}\sqrt{\frac{R_{\text{src}} + R_{\text{bkg}}}{T}} \tag{9}$$

The last thing to do is to perform polarimetric sensitivity calculations for Daksha, to estimate what the MDP might be for different source strengths and angles, to get an idea of what the detection capabilities of Daksha might be like when it is fully operational.

We expect to perform these MDP calculations on our simulated GRBs in May. All these will constitute the polarization paper we aim to submit by the end of that month.

5.4 Conclusion and Acknowledgements

Huge thanks to all my teammates on the Daksha team - in particular Dr. Suman Bala, Dr. Sourav Palit, Soumya Gupta, Divita Saraogi and Sujay Mate. They've been super helpful in handling my relative inexperience in this field, and have always been ready to clear any doubts I may have had.

Dr. Suman Bala has been my direct guides ever since I took up this project, and have been, and will be instrumental to a successful Daksha mission. Thanks immensely as well, to my project advisor Prof. Varun Bhalerao, who's been leading and guiding the entire Daksha team every step of the way. I hope we'll do good work in the second part of this B.Tech Project as well, and I shall be able to make a tiny contribution to this exciting space mission!

6 Appendix

These figures are put here for the sake of completion. These are the Modulation Curves obtained for 100% polarized beams for different local sky PAs for each face. These were simulated to obtain the fitted ϕ_0 for different PA values for the plots we saw in Section 4. These were also used to obtain the μ_{100} values that we used to recover the PF for our simulated histograms. The plots are self-explanatory and are put here without further comment.

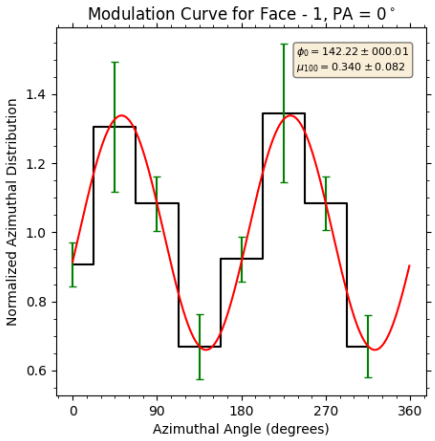

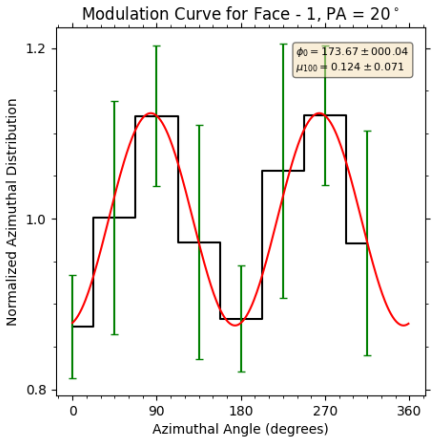

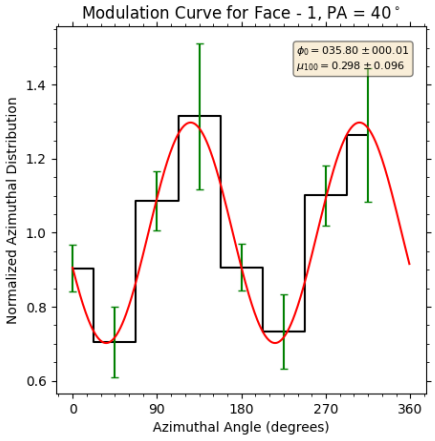

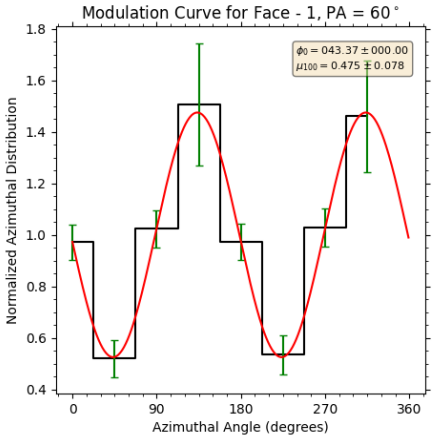

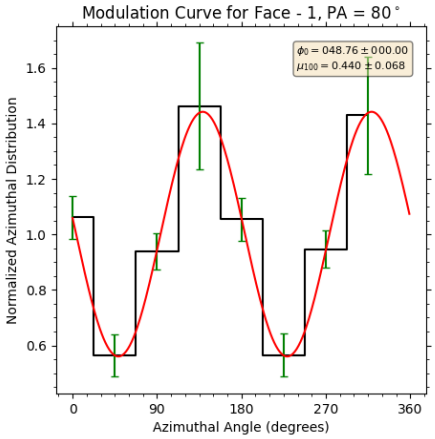
Modulation Curve for Face - 1, PA = 80°
$\phi_0 = 048.76 \pm 000.00$
$\mu_{100} = 0.440 \pm 0.068$
Normalized Azimuthal Distribution
Azimuthal Angle (degrees)

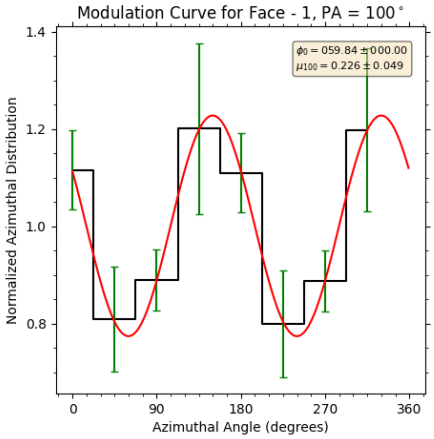
Modulation Curve for Face - 1, PA = 100°
$\phi_0 = 059.84 \pm 000.00$
$\mu_{100} = 0.226 \pm 0.049$
Normalized Azimuthal Distribution
Azimuthal Angle (degrees)

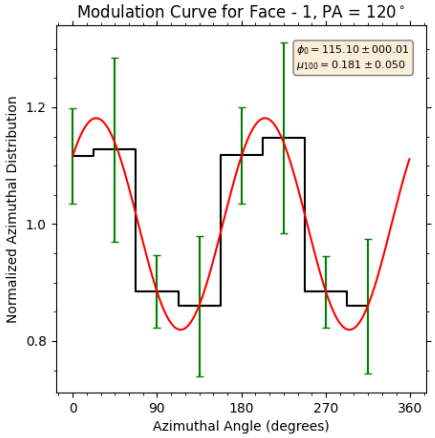
Modulation Curve for Face - 1, PA = 120°
$\phi_0 = 115.10 \pm 000.01$
$\mu_{100} = 0.181 \pm 0.050$
Normalized Azimuthal Distribution
Azimuthal Angle (degrees)

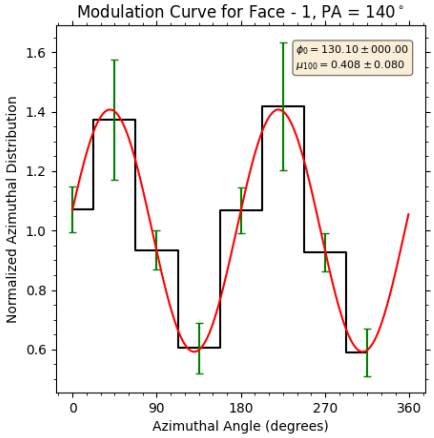
Modulation Curve for Face - 1, PA = 140°
$\phi_0 = 130.10 \pm 000.00$
$\mu_{100} = 0.408 \pm 0.080$
Normalized Azimuthal Distribution
Azimuthal Angle (degrees)

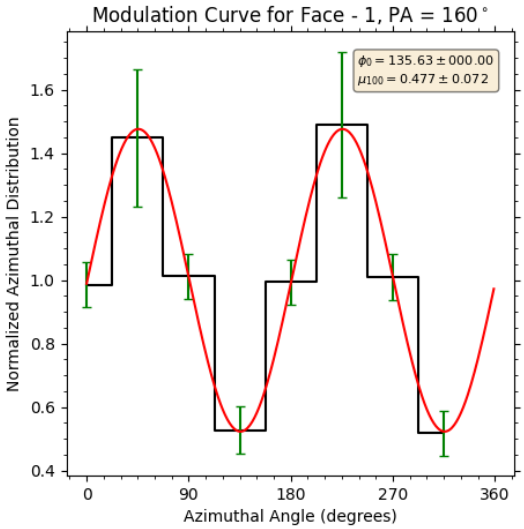
Modulation Curve for Face - 1, PA = 160 °
$\phi_0 = 135.63 \pm 000.00$
$\mu_{100} = 0.477 \pm 0.072$
Normalized Azimuthal Distribution
Azimuthal Angle (degrees)

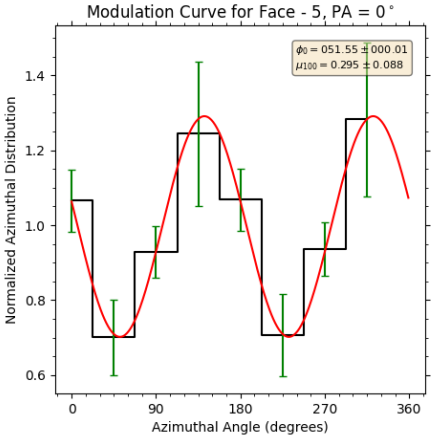
Modulation Curve for Face - 5, PA = 0 °
$\phi_0 = 051.55 \pm 000.01$
$\mu_{100} = 0.295 \pm 0.088$
Normalized Azimuthal Distribution
Azimuthal Angle (degrees)

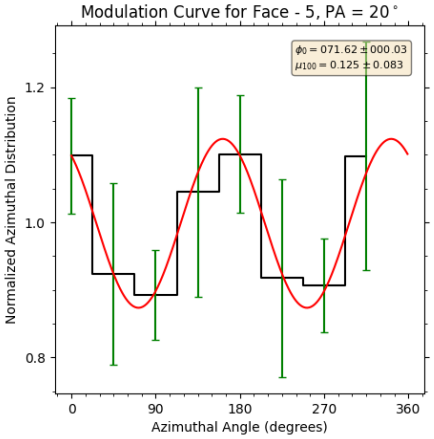
Modulation Curve for Face - 5, PA = 20 °
$\phi_0 = 071.62 \pm 000.03$
$\mu_{100} = 0.125 \pm 0.083$
Normalized Azimuthal Distribution
Azimuthal Angle (degrees)

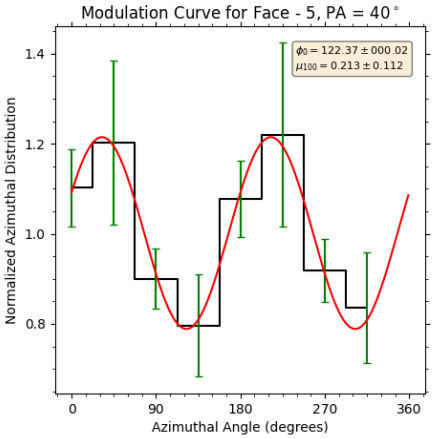
Modulation Curve for Face - 5, PA = 40°
$\phi_0 = 122.37 \pm 000.02$
$\mu_{100} = 0.213 \pm 0.112$
Normalized Azimuthal Distribution
Azimuthal Angle (degrees)

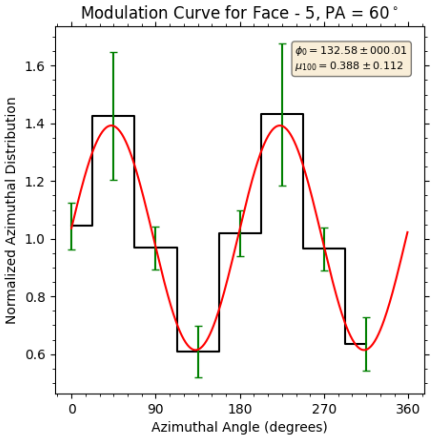
Modulation Curve for Face - 5, PA = 60°
$\phi_0 = 132.58 \pm 000.01$
$\mu_{100} = 0.388 \pm 0.112$
Normalized Azimuthal Distribution
Azimuthal Angle (degrees)

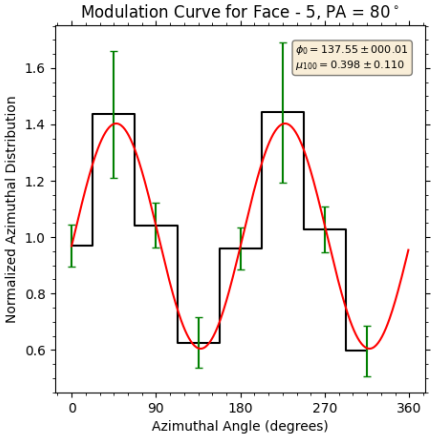
Modulation Curve for Face - 5, PA = 80°
$\phi_0 = 137.55 \pm 000.01$
$\mu_{100} = 0.398 \pm 0.110$
Normalized Azimuthal Distribution
Azimuthal Angle (degrees)

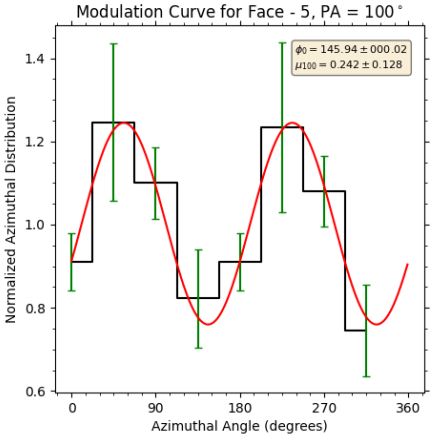
Modulation Curve for Face - 5, PA = 100°
$\phi_0 = 145.94 \pm 000.02$
$\mu_{100} = 0.242 \pm 0.128$
Normalized Azimuthal Distribution
Azimuthal Angle (degrees)

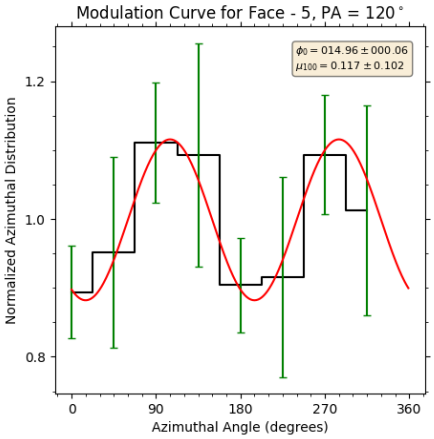
Modulation Curve for Face - 5, PA = 120°
$\phi_0 = 014.96 \pm 000.06$
$\mu_{100} = 0.117 \pm 0.102$
Normalized Azimuthal Distribution
Azimuthal Angle (degrees)

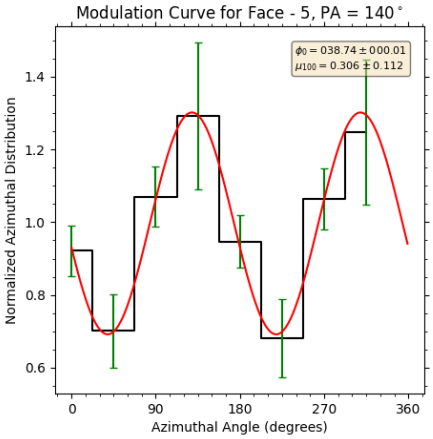
Modulation Curve for Face - 5, PA = 140°
$\phi_0 = 038.74 \pm 000.01$
$\mu_{100} = 0.306 \pm 0.112$
Normalized Azimuthal Distribution
Azimuthal Angle (degrees)

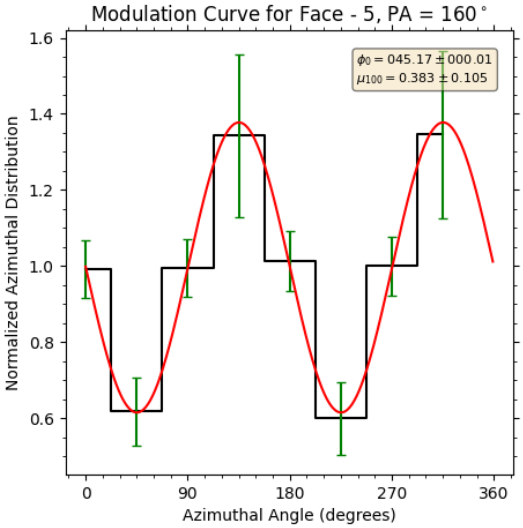
Modulation Curve for Face - 5, PA = 160°
$\phi_0 = 045.17 \pm 000.01$
$\mu_{100} = 0.383 \pm 0.105$
Normalized Azimuthal Distribution
Azimuthal Angle (degrees)

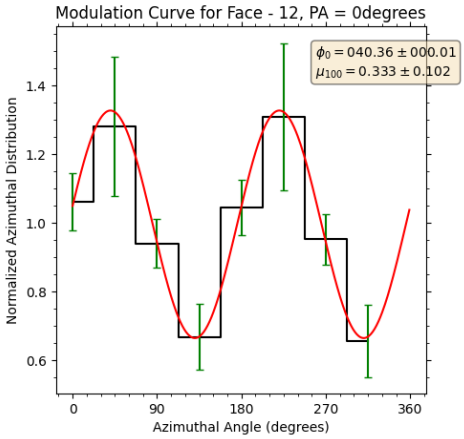
Modulation Curve for Face - 12, PA = 0degrees
$\phi_0 = 040.36 \pm 000.01$
$\mu_{100} = 0.333 \pm 0.102$
Normalized Azimuthal Distribution
Azimuthal Angle (degrees)

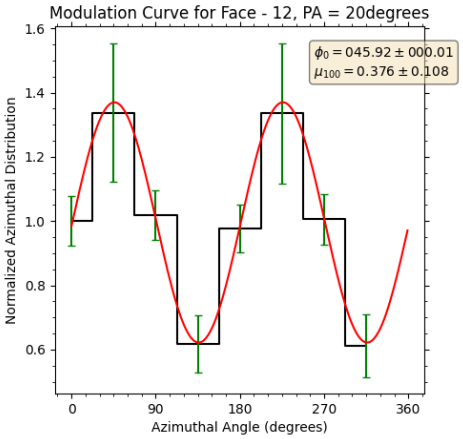
Modulation Curve for Face - 12, PA = 20degrees
$\phi_0 = 045.92 \pm 000.01$
$\mu_{100} = 0.376 \pm 0.108$
Normalized Azimuthal Distribution
Azimuthal Angle (degrees)

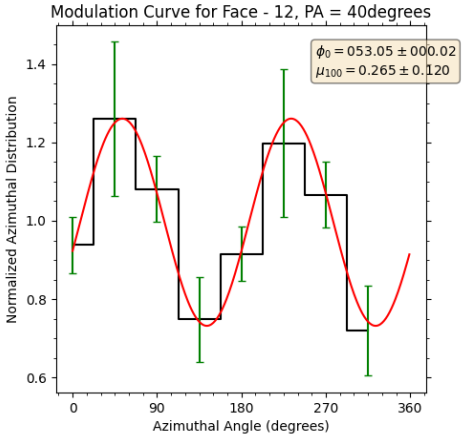
Modulation Curve for Face - 12, PA = 40degrees
$\phi_0 = 053.05 \pm 000.02$
$\mu_{100} = 0.265 \pm 0.120$
Normalized Azimuthal Distribution
Azimuthal Angle (degrees)

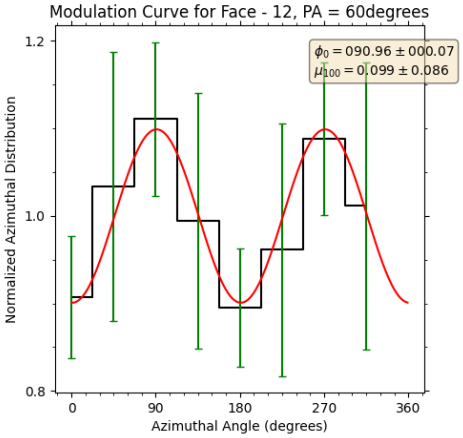
Modulation Curve for Face - 12, PA = 60degrees
$\phi_0 = 090.96 \pm 000.07$
$\mu_{100} = 0.099 \pm 0.086$
Normalized Azimuthal Distribution
Azimuthal Angle (degrees)

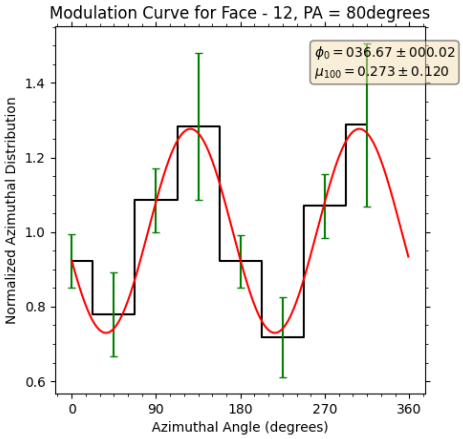
Modulation Curve for Face - 12, PA = 80degrees
$\phi_0 = 036.67 \pm 000.02$
$\mu_{100} = 0.273 \pm 0.120$
Normalized Azimuthal Distribution
Azimuthal Angle (degrees)

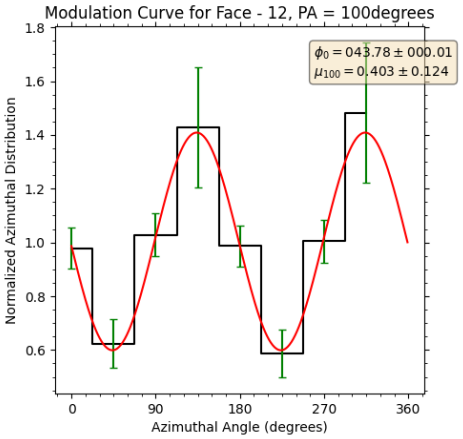
Modulation Curve for Face - 12, PA = 100degrees
$\phi_0 = 043.78 \pm 000.01$
$\mu_{100} = 0.403 \pm 0.124$
Normalized Azimuthal Distribution
Azimuthal Angle (degrees)

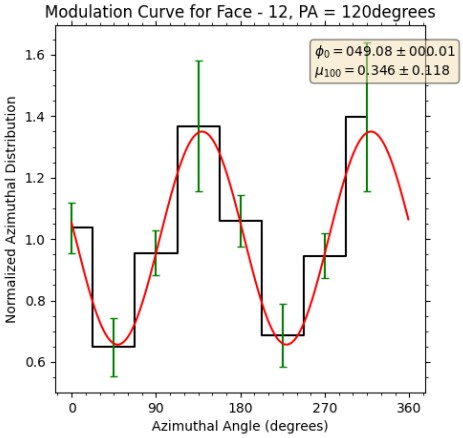
Modulation Curve for Face - 12, PA = 120degrees
$\phi_0 = 049.08 \pm 000.01$
$\mu_{100} = 0.346 \pm 0.118$
Normalized Azimuthal Distribution
Azimuthal Angle (degrees)

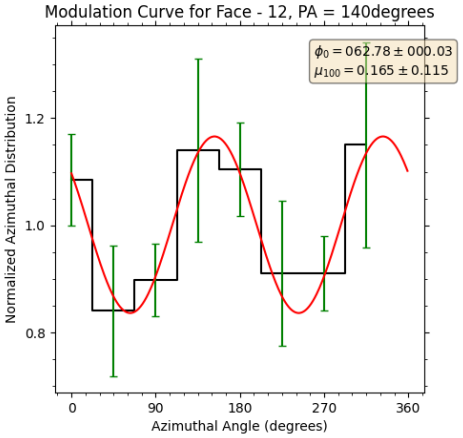
Modulation Curve for Face - 12, PA = 140degrees
$\phi_0 = 062.78 \pm 000.03$
$\mu_{100} = 0.165 \pm 0.115$
Normalized Azimuthal Distribution
Azimuthal Angle (degrees)

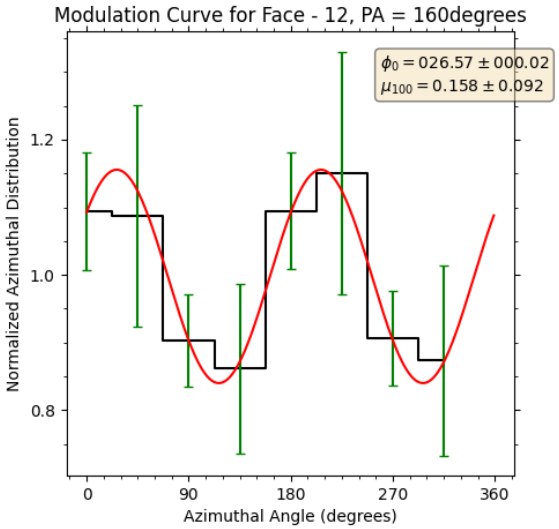

References

[1] Philip Kaaret. *X-Ray Polarimetry*. 2016. arXiv: 1408.5899 [astro-ph.IM].

[2] ESO. *Transparency of the atmosphere*. 2010. URL: https://www.eso.org/public/images/atm_opacity/ (visited on 25/11/2021).

[3] Boris E. Stern and Juri Poutanen. 'Gamma-ray bursts from synchrotron self-Compton emission'. In: *Monthly Notices of the Royal Astronomical Society* 352.3 (Aug. 2004), L35–L39. ISSN: 0035-8711. DOI: 10.1111/j.1365-2966.2004.08163.x. URL: http://dx.doi.org/10.1111/j.1365-2966.2004.08163.x.

[4] S. V. Vadawale et al. 'Hard X-ray polarimetry with Astrosat-CZTI'. In: *Astronomy & Astrophysics* 578 (June 2015), A73. DOI: 10.1051/0004-6361/201525686. URL: https://doi.org/10.1051/0004-6361/201525686.

[5] V. Bhalerao et al. 'The Cadmium Zinc Telluride Imager on AstroSat'. In: *Journal of Astrophysics and Astronomy* 38.2 (June 2017). DOI: 10.1007/s12036-017-9447-8. URL: https://doi.org/10.1007/s12036-017-9447-8.

[6] Robert Novick. 'Stellar And Solar X-Ray Polarimetry'. In: *Optical Engineering* 20.1 (Feb. 1981). DOI: 10.1117/12.7972658. URL: https://doi.org/10.1117/12.7972658.

[7] F. Lei, A. J. Dean and G. L. Hills. In: *Space Science Reviews* 82.3/4 (1997), pp. 309–388. DOI: 10.1023/a:1005027107614. URL: https://doi.org/10.1023/a:1005027107614.

[8] R. Novick et al. 'Polarization of Cosmic X-Ray Sources'. In: *Annals of the New York Academy of Sciences* 302 (1977).

[9] Martin C. Weisskopf, Ronald F. Elsner and Stephen L. O'Dell. 'On understanding the figures of merit for detection and measurement of x-ray polarization'. In: *Space Telescopes and Instrumentation 2010: Ultraviolet to Gamma Ray* (July 2010). DOI: 10.1117/12.857357. URL: http://dx.doi.org/10.1117/12.857357.

[10] Stefano Del Sordo et al. 'Progress in the Development of CdTe and CdZnTe Semiconductor Radiation Detectors for Astrophysical and Medical Applications'. In: *Sensors* 9.5 (May 2009), pp. 3491–3526. DOI: 10.3390/s90503491. URL: https://doi.org/10.3390/s90503491.

[11] Tanmoy Chattopadhyay. 'Observational Aspects of Hard X-ray Polarimetry'. In: (2016). DOI: 10.5281/ZENODO.50640. URL: https://zenodo.org/record/50640.

[12] S. Agostinelli et al. 'Geant4—a simulation toolkit'. In: *Nuclear Instruments and Methods in Physics Research Section A: Accelerators, Spectrometers, Detectors and Associated Equipment* 506.3 (July 2003), pp. 250–303. DOI: 10.1016/s0168-9002(03)01368-8. URL: https://doi.org/10.1016/s0168-9002(03)01368-8.

[13] Sujay Mate et al. 'The AstroSat mass model: Imaging and flux studies of off-axis sources with CZTI'. In: *Journal of Astrophysics and Astronomy* 42.2 (Aug. 2021). ISSN: 0973-7758. DOI: 10.1007/s12036-021-09763-x. URL: http://dx.doi.org/10.1007/s12036-021-09763-x.

[14] Tanmoy Chattopadhyay et al. 'Prompt Emission Polarimetry of Gamma-Ray Bursts with the AstroSat CZT Imager'. In: *The Astrophysical Journal* 884.2 (Oct. 2019), p. 123. DOI: 10.3847/1538-4357/ab40b7. URL: https://doi.org/10.3847/1538-4357/ab40b7.

[15] Kenji Toma et al. 'STATISTICAL PROPERTIES OF GAMMA-RAY BURST POLARIZATION'. In: *The Astrophysical Journal* 698.2 (May 2009), pp. 1042–1053. DOI: 10.1088/0004-637x/698/2/1042. URL: https://doi.org/10.1088/0004-637x/698/2/1042.